ACS Photonics

Article

pubs.acs.org/journal/apchd5

Interaction Effects between Magnetic and Chiral Building Blocks: A New Route for Tunable Magneto-chiral Plasmonic Structures

Gaspar Armelles,*[,†] Alfonso Cebollada,[†] Hua Yu Feng,[†,‡] Antonio García-Martín,[†] David Meneses-Rodríguez,[†] Jun Zhao,[§] and Harald Giessen[§]

[†]IMM-Instituto de Microelectrónica de Madrid (CNM-CSIC), Isaac Newton 8, PTM, E-28760, Tres Cantos, Madrid, Spain

[‡]IMDEA Nanoscience, Faraday 9, Ciudad Universitaria de Cantoblanco, 28049, Madrid, Spain

[§]4th Physics Institute and Research Center SCoPE, University of Stuttgart, Pfaffenwaldring 57, 70569, Stuttgart, Germany

Supporting Information

ABSTRACT: We propose a novel active magneto-chiral system consisting of a separated Au/Co multilayer with perpendicular magnetic anisotropy and plasmonic chiral oligomers. The electromagnetic interaction between the Au/Co multilayer and chiral building blocks, which is governed by their separation distance, plays a relevant role in the control of both magneto-optical and chiral activity, resulting in a strong effect on the chiro-optical response. Due to the interaction-induced detuning of the disk resonances in the oligomers, the chiro-optical activity decreases with increasing interaction strength. The possibility to tune both magneto- and chiro-optical properties of the system by controlling the interaction strength opens the door for the fabrication of magneto-chiral systems in a wide spectral range, which is determined by both constituting magnetic and chiral components, as well as their electromagnetic interaction.

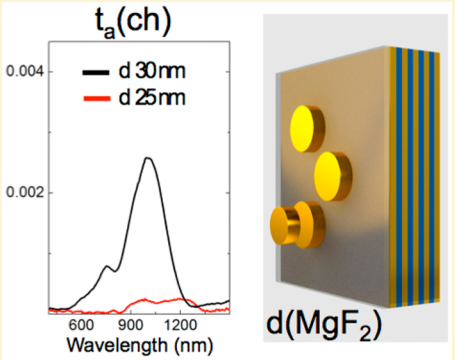

KEYWORDS: *chiral, magneto-optics, plasmons, circular dichroism, optical activity*

Chirality is one of the most fascinating aspects of optics, comprising nanostructures whose mirror images cannot be superposed onto themselves. A convenient way to detect the chirality of a nanostructure is to analyze its optical response and determine whether it depends on the handedness of the impinging light, i.e., to measure its chiro-optical effect. In natural elements, the intensity of such a chiro-optical effect is usually small, but lately a new family of chiral media based on metal−dielectric nanostructures, which exhibits enhancement of the chiro-optical activity, has been proposed.[1−7] These structures have found applications in different areas, such as negative refractive index materials,[8] asymmetric transmission,[9] or broadband circular polarizers.[10,11] Recently, it has been put forward that ultrasensitive detection of chiral molecules can be achieved using artificial chiral metallic nanostructures.[12,13] In addition, several approaches for active control of chirality have also been considered, such as reconfigurable 3D plasmonic metamolecules[14,15] or photoactive chiral metamaterials.[16−18]

On the other hand, circularly polarized light traversing a magneto-optical (MO)-active medium experiences a similar effect as that when traversing a chiral medium. Therefore, applying an external magnetic field offers a natural way to control light propagation in chiral structures. Thus, magneto-chiral structures have been fabricated using ferromagnetic or magneto-plasmonic layers, being a promising route for the development of new strategies for chiro-optical sensing.[19,20] Moreover, theoretical works on magneto-chiral structures have predicted exciting phenomena, such as nonreciprocal dispersion relation or backward wave propagating eigenmodes, with potential for use in telecom applications.[21−30]

Within this context, exploring novel systems that exploit the strong relationship between MO activity and chirality is of obvious interest. *In this work we propose a new concept of magneto-chiral systems, in which the magnetic and chiral components are spatially separated, so that it is possible to control their mutual interaction.*

RESULTS AND DISCUSSION

For that purpose, two elements, one MO active and the other chiral, are placed nearby and separated by a dielectric spacer of variable thickness, therefore giving rise to a compound system with tunable magneto-optical and chiro-optical activity (see Figure 1). As an MO-active structure we have used a 4 × (3 nm Au/1.1 nm Co) multilayer. For this specific Co thickness, the system exhibits perpendicular magnetic anisotropy, allowing magnetic saturation along the surface normal with relatively small magnetic fields.[31] This way, because of the MO character of the Co layer when magnetized along the propagation direction of the light, the transmission depends on the handedness of the light. On the other hand, the chiro-optical building block can be selected considering two different approaches: either by using structures with chiral shapes or

Received: March 27, 2015
Published: August 17, 2015

DOI: 10.1021/acsphotonics.5b00158
ACS Photonics 2015, 2, 1272−1277

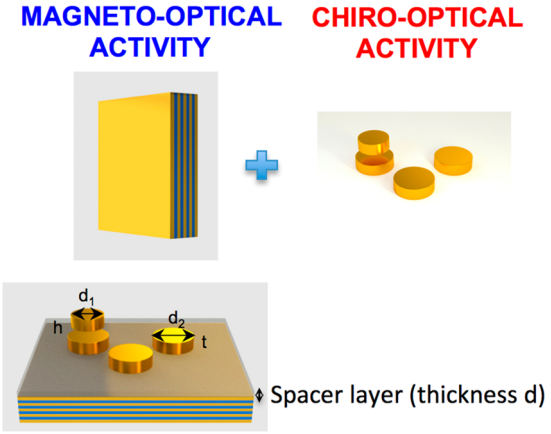

Figure 1. System with simultaneous magneto-optical activity and chiro-optical activity (bottom) obtained by placing a Au/Co multilayer (top left) underneath 3D chiral plasmonic oligomers (top right). d_1 = 140 nm, d_2 = 220 nm, t = 15 nm, and h = 25 nm define the size parameters of the elements of the oligomer. The electromagnetic interaction between these two components is controlled by the thickness d of a dielectric spacer layer (in this case MgF_2).

by placing achiral nanostructures in a chiral arrangement. In the second case the chiro-optical properties appear as the result of the electromagnetic interaction between the nanostructures, and these arrangements can be viewed as chiral metamolecules. In this work, we have used the second approach, namely, chiral Au oligomers as a chiro-optical building block.[6,7] In this specific case the oligomer is constituted by three Au nanodisks of 15 nm thickness (t) and 220 nm diameter (d_2) in a right-angle configuration with a 250 nm center-to-center distance. On top of one of the nanodisks (see Figure 1) an additional Au nanodisk that is 15 nm thick (t) and 140 nm in diameter (d_1) is deposited with a 25 nm thick MgF_2 spacer (h).

In Figure 2a we present a differential transmission spectrum of right-handed and left-handed circularly polarized light (divided by the sum of the transmission) for the MO building block measured in magnetic saturation. The spectrum consists of a broad dip, whose intensity increases with the thickness of the Co layer (not shown). This enhancement is conditioned by the fact that increasing the thickness of the Co layer directly implies increasing of the magnetic field that saturates the structure perpendicularly to its surface plane (see Supporting Information). The MO building block selected for this work represents a trade-off between both sizable MO activity and low saturation magnetic fields along the surface normal.

On the other hand, the same magnitude for the chiral building block (no magnetic field is applied in this case) is shown in Figure 2b. As it can be seen, these structures show multiple resonances in the visible and near-infrared range that are related to different plasmon modes of the Au oligomers and have large chiro-optical signals.

Therefore, using these two systems as MO-active and chiral building blocks, our magneto-chiral compound system will be formed by the MO and chiro-optical building blocks separated by a thin dielectric MgF_2 spacer, which allows controlling the mutual interaction.

These complex structures are fabricated in a three-step process. The MO building block is first deposited by thermal evaporation in ultrahigh vacuum on glass substrates, and afterward the MgF_2 spacer is deposited by electron-gun evaporation. Finally, the chiro-optical building block is

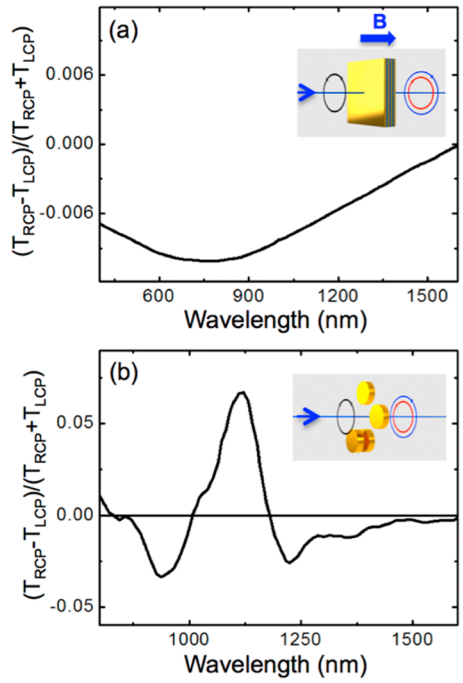

Figure 2. (a) Difference in transmission for right-handed and left-handed circularly polarized light for a magnetically saturated Au/Co multilayer. (b) Difference in transmission for right-handed and left-handed circularly polarized light for 3D chiral plasmonic oligomers (ref 6).

fabricated using hole−mask colloidal lithography[32,33] combined with tilted-angle rotation evaporation.[34] A representative AFM image of the final structures with both building blocks in place is shown in Figure 3a.

The spacer thickness dependence of the interaction between these two building blocks is illustrated in Figure 3b, where we present theoretical simulations of the transmission spectra of a Au/Co multilayer as well as of the complete system made of oligomers separated from a Au/Co multilayer by a dielectric spacer for different spacer thicknesses, using periodic boundary conditions (see Supporting Information for further details). The multilayer spectrum shows a monotonic decrease of the transmission with increasing wavelength, whereas the spectrum of the complete structure shows, superimposed to the Au/Co multilayer curve, a structured dip, or s-like structure, originating from the oligomers. As the thickness of the MgF_2 layer is reduced, the oligomer-related structure shows a clear red-shift. The small structure at ∼1100 nm results from a diffraction order appearing in the substrate due to the periodic boundary conditions employed in the calculation. On the other hand, in Figure 3c we present the experimental unpolarized transmission spectra of a Au/Co multilayer and of two complete structures with 30 and 25 nm thick MgF_2 spacers, respectively. The spectral features observed in the simulations are also present in the experiments, with the typical broadening arising from fabrication and nanostructure defects, as well as the red-shift as the spacer layer gets thinner. This thickness dependence of the oligomer-related structure observed in both the theoretical simulations and the experimental results is due to the enhanced interaction between the oligomers and the Au/Co multilayer, as previously observed for plasmon resonances of Au or Ag nanoparticles on top of a metallic substrate with a dielectric spacer in between.[35−38]

DOI: 10.1021/acsphotonics.5b00158
ACS Photonics 2015, 2, 1272−1277

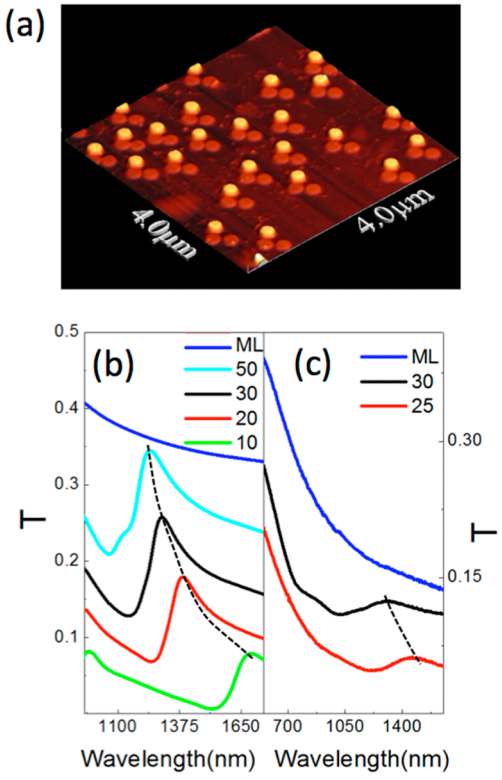

Figure 3. (a) AFM image of the compound structure, where the 3D chiral oligomers have been deposited onto the MgF_2 spacer/(Au/Co multilayer). (b) Theoretical simulation of the unpolarized transmission for a Au/Co multilayer (blue curve) and for a periodic array of oligomers separated from a Au/Co multilayer by a dielectric spacer, for different spacer thicknesses. (c) Experimental transmission for unpolarized light of a representative Au/Co multilayer (blue curve) and for two structures with different MgF_2 spacer thicknesses: black curve 30 nm, red curve 25 nm. For clarity, all curves, theoretical and experimental, have been vertically displaced.

After confirming that the spacer thickness actually modifies the interaction between the MO and chiro-optical building blocks, the next step is to explore their collective magneto-chiral behavior in the presence of an external magnetic field. It has to be taken into account that, due to the spatial arrangement of the oligomer structures, the systems exhibit not only MO and chiro-optical properties but also in-plane optical anisotropy.[6,33] For this reason, and to discern from an experimental point of view the different contributions to the MO and optical properties of the systems, generalized ellipsometry measurements (see Supporting Information) have been carried out. These measurements allow the discrimination of different ratios of the coefficients in the transmission Jones matrix:

$$\begin{pmatrix} t_{xx} & t_{xy} \\ t_{yx} & t_{yy} \end{pmatrix} \tag{1}$$

If the system has no in-plane optical anisotropy, the difference in the transmission for right-handed and left-handed circularly polarized light can be related to the transmission Jones matrix's coefficients as

$$\Delta T = \frac{I_{RCP} - I_{LCP}}{I_{RCP} + I_{LCP}} = 2\mathrm{Im}\left(\frac{t_{xy}}{t}\right) \tag{2}$$

with $t = t_{xx} = t_{yy}$ and $t_{xy} = -t_{yx}$ (we have assumed $t_{xy} \ll t$).

However, if the system has in-plane optical anisotropy, it is necessary to decompose t_{xy} (t_{yx}) into its symmetric ($t_{sy} = (t_{xy} + t_{yx})/2$) and antisymmetric ($t_a = (t_{xy} - t_{yx})/2$) components. The symmetric part (t_{sy}) is related to the in-plane optical anisotropy, whereas the antisymmetric component (t_a) is related to both the chiro-optical (t_{ch}) and MO activities (t_{MO}): $t_a = t_{ch} \pm t_{MO}M$, with M being the normalized magnetization of the structure along the surface normal. Then, the transmission matrix can be rewritten as

$$\begin{pmatrix} t_{xx} & t_{sy} + t_a \\ t_{sy} - t_a & t_{yy} \end{pmatrix} \tag{3}$$

Following the relationship between the difference in the transmission for right-handed and left-handed circularly polarized light and the imaginary component of t_{xy}/t, it is possible to consider instead a ΔT_A ($\Delta T_A = \mathrm{Im}(t_a/t_{yy})$) that permits discerning contributions of chiro-optical character from those of MO nature.

The spectral dependence of ΔT_A obtained for the two spacer thicknesses experimentally considered is presented in Figure 4a and d with the Co layers fully magnetized along the positive and negative direction. For the sample with a thicker MgF_2 spacer, two distinct features are observed and located in the spectral regions of the two resonances as shown in Figure 3c, whereas for the sample with a thinner MgF_2 spacer (Figure 4d), only a single feature is clearly observed in the region of the lower energy resonance. Our presented formalism allows thus separating this ΔT_A into its chiro-optical (ΔT_{Ch}) and MO (ΔT_{MO}) components, as shown in Figure 4b,c and e,f:

$$\Delta T_{Ch} = \frac{1}{2}\left\{\mathrm{Im}\left(\frac{t_a(M)}{t_{yy}}\right) + \mathrm{Im}\left(\frac{t_a(-M)}{t_{yy}}\right)\right\} \tag{4}$$

and

$$\Delta T_{MO} = \frac{1}{2}\left\{\mathrm{Im}\left(\frac{t_a(M)}{t_{yy}}\right) - \mathrm{Im}\left(\frac{t_a(-M)}{t_{yy}}\right)\right\} \tag{5}$$

Obviously, it is possible to reconstruct the ΔT_A spectra for positive magnetic saturation ($+M$) by simply adding the ΔT_{Ch} and the ΔT_{MO} spectra, as well as the corresponding ΔT_A spectra for negative saturation ($-M$) by subtracting them.

The results presented in Figure 4 depend on the relative orientation of the structures with respect to the incoming beam polarization due to the mentioned in-plane optical anisotropy. The experimental and theoretical simulations of the orientation-independent chiro-optical and MO fingerprints, i.e., the modulus of the different components of t_a (see Supporting Information), are depicted in Figure 5. The effect of the interaction between the oligomers and the Au/Co multilayer is clearly seen. For example, in Figure 5a and b we present the theoretical simulation and experimental t_{MO} spectra for the same structures considered in Figure 3. The effect of placing the oligomers on top of the ML (Figure 5a,b) is similar to that observed for the transmission spectra: the appearance of a broad dip, or s-like shaped structure, whose position shifts toward lower energy as we decrease the spacer layer thickness. Since the MO activity is basically proportional to the EM field in the MO-active region (the ML),[39−41] this modification of the MO intensity indicates that the oligomer−ML interaction

DOI: 10.1021/acsphotonics.5b00158
ACS Photonics 2015, 2, 1272−1277

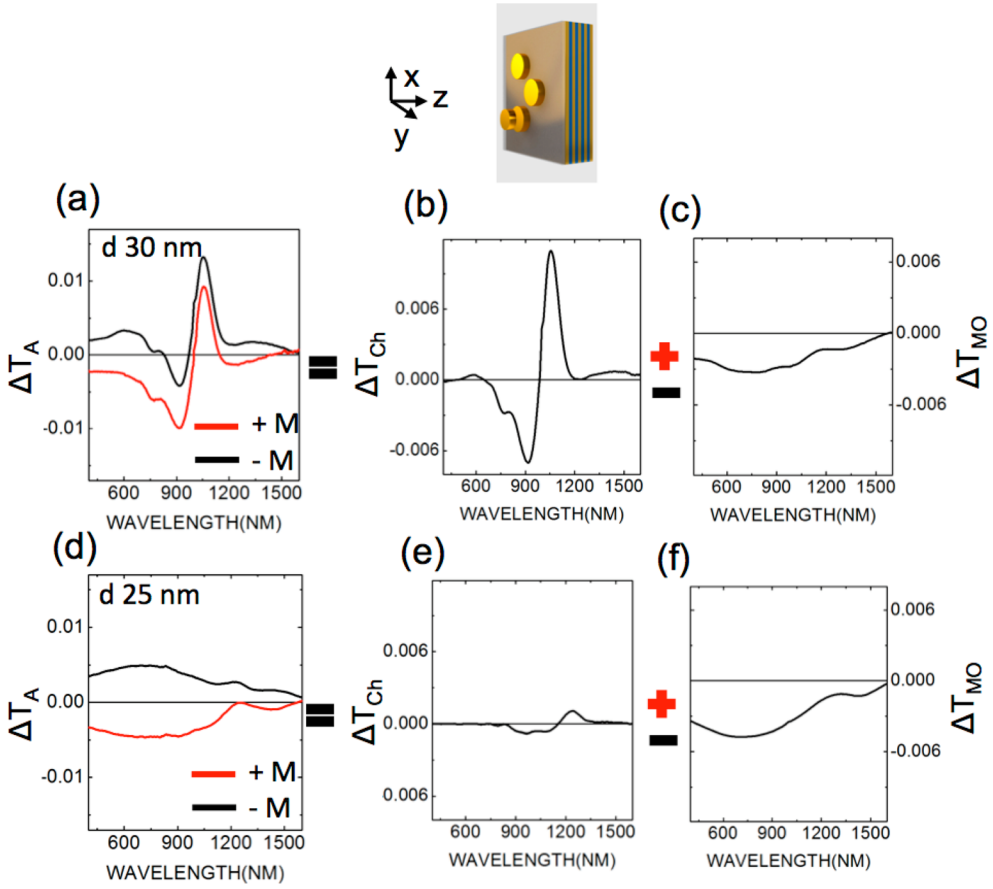

Figure 4. Decomposition of ΔT_A (a and d) into its chiral ΔT_{Ch} (b and e) and magneto-optical ΔT_{MO} (c and f) components for two MgF_2 spacer thicknesses, separating the purely chiral and MO constituents.

produces a red-shift not only of the oligomer resonances but also of the EM field in the multilayer.

On the other hand, the effect of the interaction on the chiral contribution is much more pronounced. In Figure 5c and d we present the theoretical and experimental t_{Ch} for different spacer layer thicknesses. The theoretical spectra (Figure 5d) exhibit a main feature located in the spectral region of the oligomer resonances, a feature that red-shifts as the spacer thickness is reduced. Secondary features observed in the high-energy side are due to the periodic arrangement of the oligomers in the simulation. A similar behavior is observed in the experiment, with the appearance of a feature related to the oligomer resonance and that red-shifts as the MgF_2 spacer gets thinner. Again the features are broader and somehow weaker than in the theoretical simulation probably due to fabrication and grain structure defects. Additionally, there is a strong reduction of the chiro-optical activity as we reduce the spacer layer thickness. This effect can be related to the fact that the enhanced EM interaction between the ML and the oligomers is situated around the resonance frequencies of the Au disks. The chiro-optical activity originates from the EM interaction between the bottom layer disks and the top disk, which is largest for the two vertically aligned disks with the same resonance frequencies. As we detune the resonance frequencies (i.e., by using disks of different sizes), the chiro-optical activity decreases. The EM interaction between the disks and the ML depends on their different mutual distances and the different polarizability for the bottom and top disks. Therefore, the red-shift induced on the disk resonance by the interaction with the ML is different for the disks in both layers, and the detuning of their resonances increases with decreasing spacer thickness, resulting in the reduction of the chiro-optical activity.

Finally, the in-plane optical anisotropy stems mainly from the L-shaped arrangement of the bottom layer disks. These three disks have the same size, corresponding to the same EM interaction with the ML. Therefore, we should expect that the in-plane optical anisotropy depends more weakly on the spacer layer thickness than the chiro-optical activity. In Figure 5e and f we present t_{sy}, which is linked to the strength of the in-plane optical anisotropy. Apart from a red-shift of the spectrum as we decrease the MgF_2 layer thickness, the intensity of the in-plane optical anisotropy is nearly the same for all spacer thicknesses.

In conclusion, we have presented a novel system that exhibits both magneto-optical and chiro-optical activity by combining interacting magnetic Au/Co multilayers and chiral Au plasmonic oligomers. Spatially separating the two building blocks allows for tuning their electromagnetic interaction by changing their mutual distance. We have analyzed, both experimentally and theoretically, the EM interaction between the Au/Co ML and the Au oligomers and demonstrated how tuning this interaction affects both the MO and optical properties of the system.

The ML−oligomer interaction displays a stronger effect on the chiro-optical activity than on the MO activity, with a large reduction of the chiro-optical activity as we increase the oligomer−ML interaction. This reduction is attributed to the increased detuning of the Au disk resonances in the oligomers induced by the interaction. The possibility to tune both the

DOI: 10.1021/acsphotonics.5b00158
ACS Photonics 2015, 2, 1272−1277

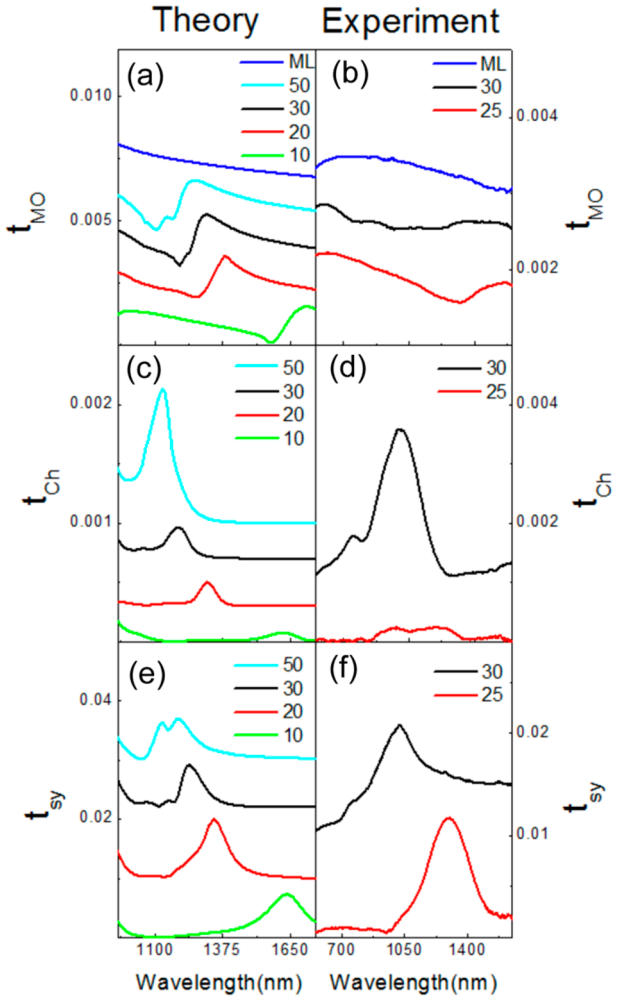

Figure 5. (a) Theoretical simulation of the MO activity (t_{MO}) for a Au/Co multilayer (blue curve) and for a periodic array of oligomers separated from a Au/Co multilayer by a dielectric spacer, for different spacer thicknesses. (b) Experimental Mo activity (t_{MO}) of a representative Au/Co multilayer (blue curve) and for two structures with different MgF_2 spacer thicknesses (black curve 30 nm, red curve, 25 nm). (c) Theoretical simulation of the chiro-optical activity (t_{Ch}) for a periodic array of oligomers separated from a Au/Co multilayer by a dielectric spacer, for different spacer thicknesses. (d) Experimental chiro-optical activity (t_{Ch}) for two structures with different MgF_2 spacer thicknesses (black curve 30 nm, red curve 25 nm). (e) Theoretical simulation of the same parameter for a periodic array of oligomers separated from a Au/Co multilayer by a dielectric spacer, for different spacer thicknesses. (f) Experimental symmetric component (t_{sy}) for the two structures with different MgF_2 spacer thicknesses. For clarity, all curves, both theoretical and experimental, have been vertically displaced. As mentioned in the text, the structure at ~1100 nm in the theoretical simulation results from a diffraction order appearing in the substrate due to the periodic boundary conditions employed in the calculation.

MO and chiro-optical properties of the system by controlling the interaction between the building blocks opens the door toward fabrication of magneto-chiral systems in a wide spectral range determined by both the constituting building blocks and their electromagnetic interaction. On the other hand, using structures whose chiro-optical properties are determined by their chiral shape, such as chiral-split resonators, should give rise to different interaction effects, thus increasing the tuning capabilities of these novel systems. Finally, chiral structures fabricated with pure ferromagnetic materials have recently shown cross-coupling effects between chirality and magnetism, giving rise to a magnetic field control of the transmission properties of unpolarized light, which depends on the direction of the light propagation.[42] As the origin of this effect is not yet completely understood, our approach offers a way to control the relative weight of the electromagnetic field intensity in the regions responsible for the chiral properties and for the magnetism, respectively, and therefore might help shed some light on the origin of the cross-coupling between chirality and magnetism in plasmonic structures.

■ ASSOCIATED CONTENT

Supporting Information

The Supporting Information is available free of charge on the ACS Publications website at DOI: 10.1021/acsphotonics.5b00158.

The magnetic behavior of Au/Co multilayers, the theoretical model used to simulate the different spectra, and the in-plane orientation dependence of the transmission Jones matrix coefficients (PDF)

■ AUTHOR INFORMATION

Corresponding Author

*E-mail: Gaspar@imm.cnm.csic.es.

Notes

The authors declare no competing financial interest.

■ ACKNOWLEDGMENTS

Funding from the Spanish Ministry of Economy and Competitiveness through grants "FUNCOAT" CONSOLIDER CSD2008-00023 and MAPS MAT2011-29194-C02-01 is acknowledged. H.Y.F. thanks the funding from CSC (Chinese Scholarship Council), grant no. 201206220112. J.Z. and H.G. acknowledge support from ERC (Complexplas), BMBF, DFG, AvH-Stiftung, Carl-Zeiss-Foundation, EU-COST (Nanospectroscopy), and MWK Baden-Württemberg.

■ REFERENCES

(1) Liu, N.; Liu, H.; Zhu, S.; Giessen, H. Stereometamaterials. *Nat. Photonics* **2009**, *3*, 157−162.

(2) Fan, Z.; Govorov, A. O. Plasmonic Circular Dichroism of Chiral Metal Nanoparticle Assemblies. *Nano Lett.* **2010**, *10*, 2580−2587.

(3) Guerrero-Martínez, A.; Alonso-Gómez, J. L.; Auguié, B.; Cid, M. M.; Liz-Marzán, L. M. From Individual to Collective Chirality in Metal Nanoparticles. *Nano Today* **2011**, *6*, 381−400.

(4) Valev, V. K.; Baumberg, J. J.; Sibilia, C.; Verbiest, T. Chirality and Chirooptical Effects in Plasmonic Nanostructures: Fundamentals, Recent Progress, and Outlook. *Adv. Mater.* **2013**, *25*, 2517−2534.

(5) Zhao, J.; Jaber, S.; Mulvaney, P.; Braun, P. V.; Giessen, H. Repetitive Hole-Mask Colloidal Lithography for the Fabrication of Large-Area Low-Cost Plasmonic Multishape Single-Layer Metasurfaces_. *Adv. Opt. Mater.* **2015**, *3*, 680.

(6) Hentschel, M.; Wu, L.; Schäferling, M.; Bai, P.; Li, E. P.; Giessen, H. Optical Properties of Chiral Three-Dimensional Plasmonic Oligomers at the Onset of Charge-Transfer Plasmons. *ACS Nano* **2012**, *6*, 10355−10365.

(7) Hentschel, M.; Schäferling, M.; Weiss, T.; Liu, N.; Giessen, H. Three-Dimensional Chiral Plasmonic Oligomers. *Nano Lett.* **2012**, *12*, 2542−2547.

(8) Pendry, J. B. A Chiral Route to Negative Refraction. *Science* **2004**, *306*, 1353−1355.

DOI: 10.1021/acsphotonics.5b00158
ACS Photonics 2015, 2, 1272−1277

(9) Li, Z.; Utlu, M.; Ozbay, E. Chiral Metamaterials: From Optical Activity and Negative Refractive Index to Asymmetric Transmission. *J. Opt.* **2013**, *15*, 023001.
(10) Gansel, J. K.; Thiel, M.; Rill, M. S.; Decker, M.; Bade, K.; Saile, V.; Von Freymann, G.; Linden, S.; Wegener, M. Gold Helix Photonic Metamaterial as Broadband Circular Polarizer. *Science* **2009**, *325*, 1513−1515.
(11) Zhao, Y.; Belkin, M. A.; Alù, A. Twisted Optical Metamaterials for Planarized Ultrathin Broadband Circular Polarizers. *Nat. Commun.* **2012**, *3*, 870.
(12) Hendry, E.; Carpy, T.; Johnston, J.; Popland, M.; Mikhaylovskiy, R. V.; Lapthorn, A. J.; Kelly, S. M.; Barron, L. D.; Gadegaard, N.; Kadodwala, M. Ultrasensitive Detection and Characterization of Biomolecules Using Superchiral Fields. *Nat. Nanotechnol.* **2010**, *5*, 783−787.
(13) Ma, W.; Kuang, H.; Xu, L.; Ding, L.; Xu, C.; Wang, L.; Kotov, N. A. Attomolar DNA Detection with Chiral Nanorod Assemblies. *Nat. Commun.* **2013**, *4*, 2689.
(14) Kuzyk, A.; Schreiber, R.; Zhang, H.; Govorov, A. O.; Liedl, T.; Liu, N. Reconfigurable 3D Plasmonic Metamolecules. *Nat. Mater.* **2014**, *13*, 862−866.
(15) Yin, X.; Schäferling, M.; Michel, A.; Tittl, A.; Wuttig, W.; Taubner, T.; Giessen, H. Active Chiral Plasmonics. *Nano Lett.* **2015**, *15*, 4255.
(16) Zhou, J.; Chowdhury, D. R.; Zhao, R.; Azad, A. K.; Chen, H.-T.; Soukoulis, C. M.; Taylor, A. J.; O'Hara, J. F. Terahertz Chiral Metamaterials With Giant and Dynamically Tunable Optical Activity. *Phys. Rev. B: Condens. Matter Mater. Phys.* **2012**, *86*, 035448.
(17) Zhang, S.; Zhou, J.; Park, Y.-S.; Rho, J.; Singh, R.; Nam, S.; Azad, A. K.; Chen, H.-T.; Yin, X.; Taylor, A. J.; et al. Photoinduced Handedness Switching in Terahertz Chiral Metamolecules. *Nat. Commun.* **2012**, *3*, 942.
(18) Zhu, Y.; Hu, X.; Chai, Z.; Yang, H.; Gong, Q. Active control of chirality in nonlinear metamaterials. *Appl. Phys. Lett.* **2015**, *106*, 091109.
(19) Valev, V. K.; Volodin, A.; Silhanek, A. V.; Gillijns, W.; De Clercq, B.; Jeyaram, Y.; Paddubrouskaya, H.; Biris, C. G.; Panoiu, N. C.; Aktsipetrov, O. A.; et al. Plasmons Reveal the Direction of Magnetization in Nickel Nanostructures. *ACS Nano* **2011**, *5*, 91−96.
(20) Armelles, G.; Caballero, B.; Prieto, P.; Garcia, F.; Cebollada, A.; Gonzalez, M. U.; Garcia-Martin, A. Magnetic Field Modulation of Chirooptical Effects in Magnetoplasmonic Structures. *Nanoscale* **2014**, *6*, 3737−3741.
(21) Engheta, N.; Jaggard, D. L.; Kowarz, M. K. Electromagnetic Waves in Faraday Chiral Media. *IEEE Trans. Antennas Propag.* **1992**, *40*, 367−374.
(22) Mackay, T. G.; Lakhtakia, A. Plane Waves with Negative Phase Velocity in Faraday Chiral Mediums. *Phys. Rev. E* **2004**, *69*, 026602.
(23) Bita, I.; Thomas, E. L. Structurally Chiral Photonic Crystals With Magneto-Optic Activity: Indirect Photonic Bandgaps, Negative Refraction, and Superprism Effects. *J. Opt. Soc. Am. B* **2005**, *22*, 1199−1210.
(24) Qiu, C. W.; Li, L. W.; Yao, H.; Zouhdi, S. Properties of Faraday Chiral Media: Green Dyadics and Negative Refraction. *Phys. Rev. B: Condens. Matter Mater. Phys.* **2006**, *74*, 115110.
(25) Shen, J. Q.; He, S. Backward Waves and Negative Refractive Indices in Gyrotropic Chiral Media. *J. Phys. A: Math. Gen.* **2006**, *39*, 457−466.
(26) Mackay, T. G.; Lakhtakia, A. Negative Reflection in a Faraday Chiral Medium. *Microwave and Optical Technology Letters* **2008**, *50*, 1368−1371.
(27) Meng, F.; Zhang, K.; Wu, Q.; Li, L. Polarization Conversion of Electromagnetic Waves by Faraday Chiral Media. *J. Appl. Phys.* **2010**, *107*, 054104.
(28) Christofi, A.; Stefanou, N. Nonreciprocal Optical Response of Helical Periodic Structures of Plasma Spheres in a Static Magnetic Field. *Phys. Rev. B: Condens. Matter Mater. Phys.* **2013**, *87*, 115125.
(29) Christofi, A.; Stefanou, N. Strong Magnetochiral Dichroism of Helical Structures of Garnets Particles. *Opt. Lett.* **2013**, *38*, 4629−4631.
(30) Gao, M. X.; Guo, B.; Peng, L.; Cai, X. Dispersion Relations for Electromagnetic Wave Propagation in Chiral Plasmas. *Phys. Plasmas* **2014**, *21*, 114501.
(31) Wiedmann, M. H.; Engel, G. N.; Van Leeuwen, R. A.; Mibu, K.; Shinjo, T.; Falco, C. M. Anomalous Perpendicular Anisotropy in ultrathin Co Films. *MRS Online Proc. Libr.* **1993**, *313*, 531.
(32) Fredriksson, H.; Alaverdyan, Y.; Dmitriev, A.; Langhammer, C.; Sutherland, D. S.; Zäch, M.; Kasemo, B. Hole-MaskColloidal Lithography. *Adv. Mater.* **2007**, *19*, 4297−4302.
(33) Cataldo, S.; Zhao, J.; Neubrech, F.; Frank, B.; Zhang, C.; Braun, P. V.; Giessen, H. Hole-Mask Colloidal Nanolithography for Large-Area Low-Cost Metamaterials and Antenna-Assisted Surface-Enhanced Infrared Absorption Substrates. *ACS Nano* **2012**, *6*, 979−985.
(34) Frank, B.; Yin, X.; Schäferling, M.; Zhao, J.; Hein, S. M.; Braun, P. V.; Giessen, H. Large-area 3D Chiral Plasmonic Structures. *ACS Nano* **2013**, *7*, 6321−6329.
(35) Holland, W. R.; Hall, D. G. Frequency-Shifts of an Electric-Dipole Resonance Near a Conducting Surface. *Phys. Rev. Lett.* **1984**, *52*, 1041−1044.
(36) Leveque, G.; Martin, O. Optical Interactions in a Plasmonic Particle Coupled to a Metallic Film. *Opt. Express* **2006**, *14*, 9971−9981.
(37) Armelles, G.; Gonzalez-Diaz, J. B.; Garcia-Martin, A.; Garcia-Martin, J. M.; Cebollada, A.; Gonzalez, M. U.; Acimovic, S.; Cesario, J.; Quidant, R.; Badenes, G. Localized Surface Plasmon Resonance Effects on the Magneto-Optical Activity of Continuous Au/Co/Au Trilayers. *Opt. Express* **2008**, *16*, 16104−16112.
(38) Liu, N.; Guo, H.; Fu, L.; Schweizer, H.; Kaiser, S.; Giessen, H. Plasmon Hybridization in Stacked Cut-Wire Metamaterials. *Adv. Mater.* **2007**, *19*, 3628−3632.
(39) Temnov, V. V.; Armelles, G.; Woggon, U.; Guzatov, D.; Cebollada, A.; García-Martín, A.; García-Martín, J. M.; Thomay, T.; Leitenstorfer, A.; Bratschitsch, R. Active Magneto-Plasmonics in Hybrid Metal-Ferromagnet Structures. *Nat. Photonics* **2010**, *4*, 107−111.
(40) Meneses-Rodríguez, D.; Ferreiro-Vila, E.; Prieto, P.; Anguita, J.; González, M. U.; García-Martín, J. M.; Cebollada, A.; García-Martín, A.; Armelles, G. Probing the Electromagnetic Field Distribution within a Metallic Nanodisk. *Small* **2011**, *7*, 3317−3323.
(41) Armelles, G.; Cebollada, A.; Garcia-Martin, A.; Gonzalez, M. Magnetoplasmonics: Combining Magnetic and Plasmonic Functionalities. *Adv. Opt. Mater.* **2013**, *1*, 10−35.
(42) Eslami, S.; Gibbs, J. G.; Rechkemmer, Y.; van Slageren, J.; Alarcon-Correa, M.; Lee, T. C.; Mark, A. G.; Rikken, G. L. J. A.; Fischer, P. Chiral Nanomagnets. *ACS Photonics* **2014**, *1*, 1231−1236.

DOI: 10.1021/acsphotonics.5b00158
ACS Photonics 2015, 2, 1272−1277